Smart Structures and Systems, *Vol. 28, No. 6 (2021) 727-735*
https://doi.org/10.12989/sss.2021.28.6.727

Time dependent numerical simulation of MFL coil sensor for metal damage detection

Ali Azad [1a], Jong-Jae Lee [1b] and Namgyu Kim*[2]

[1] *Department of Civil and Environmental Engineering, Sejong University, 209, Neungdong-ro, Gwangjin-gu, Seoul, 05006, Republic of Korea*
[2] *Department of Structural Engineering Research, Korea Institute of Civil Engineering and Building Technology, 283, Goyangdae-ro, Ilsanseo-gu, Goyang-si, Gyeonggi-do, 10223, Republic of Korea*

(*Received August 13, 2019, Revised May 13, 2021, Accepted September 24, 2021*)

Abstract. Recently, non-destructive health monitoring methods such as magnetic flux leakage (MFL) method, have become popular due to their advantages over destructive methods. Currently, numerical study on this field has been limited to simplified studies by only obtaining MFL instead of induced voltage inside coil sensor. In this study, it was proposed to perform a novel numerical simulation of MFL's coil sensor by considering vital parameters including specimen's motion with constant velocity and saturation status of specimen in time domain. A steel-rod specimen with two stepwise cross-sectional changes (i.e., 21% and 16%) was fabricated using low carbon steel. In order to evaluate the results of numerical simulation, an experimental test was also conducted using a magnetic probe, with same size specimen and test parameters, exclusively. According to comparative results of numerical simulation and experimental test, similar signal amplitude and signal pattern were observed. Thus, proposed numerical simulation method can be used as a reliable source to check efficiency of sensor probe when different size specimens with different defects should be inspected.

Keywords: coil sensor; finite element analysis; magnetic flux leakage method; nondestructive testing; time dependent simulation

1. Introduction

In order to assess structural element's integrity, regular structural health monitoring must be performed, especially in some particular cases such as suspension bridge structures, cable-stayed bridge structures, oil and gas industries and etc., regular inspection is mandatory and essential (Feng *et al*. 2017, Iqbal *et al*. 2017, Kim and Park 2018). For instance, in cable-stayed infrastructures, almost entire load is carried by steel cables. Thus, any flaws such as cross-sectional loss, corrosion and internal breakage in cables may lead to catastrophic structural failure. Various nondestructive testing methods have, therefore, become popular on cable defect assessment due to their main advantage, which is being nondestructive test. Moreover, cable inspecting robots with mounted nondestructive testing (NDT) sensors are developed and considered as one the useful sensor setup for detecting damage in inaccessible locations (Mehrabi and Farhangdoust 2018). Although there are many available NDT methods such as visual inspection method (Elliott and Heymsfield 2003), MFL method (Wu *et al*. 2017a, Sun *et al*. 2018), guided waves method (Dai and He 2014, Garg *et al*. 2016, Jain and Sharma 2016, Wandowski *et al*. 2016), acoustic emission method (Caesarendra *et al*. 2016, Kuang *et al*. 2016, Munoz *et al*. 2016, Strantza *et al*. 2017, Banjara *et al*. 2019), eddy current testing method (Rocha *et al*. 2015, Rifai *et al*. 2017, Kim *et al*. 2018b), electromagnetic acoustic transducer (EMAT) method (Gomez *et al*. 2017), etc., these methods have their own drawbacks which may appear by changing test parameters such as specimen's geometry, conductivity, magnetization level, lift off, etc. As a result, based on the test condition, each single one of these aforementioned methods should be used in specific situation. MFL method is a robust method and capable of detecting surface and subsurface defects accurately. However, to inspect specimens with different sizes that consist of defects with different sizes and directions, instead of doing trial and error experimentally which leads to waste of time and costs, numerical study can be a reliable way to approve effectiveness of MFL sensor apparatus for any specific condition.

Wu *et al*. (2017b) mentioned that in conventional MFL testing setups, an inevitable gap which occurs by implementing a non-ferromagnetic support between sensor and specimen, reduces sensitivity of sensor. Here, the gap indicates the distance between sensor to the specimen's surface. To eliminate the unwanted lift off, they proposed a method for substituting a non-ferromagnetic support with ferromagnetic one in sensor probe. Finally, this proposed method was numerically evaluated using a simple two-dimensional (2D) stationary finite element analysis (FEA). To obtain effects of defect's depth and width on MFL signal, Kim *et al*. (2018b) fabricated a magnetic apparatus

*Corresponding author, Senior Researcher,
E-mail: namgyu.kim@kict.re.kr
[a] Postdoctoral Researcher, E-mail: aliazad052@gmail.com
[b] Professor, E-mail: jongjae@sejong.ac.kr

ISSN: 1738-1584 (Print), 1738-1991 (Online)

and conducted experimental tests based on MFL testing method. According to the results, defect's depth and width can be identified correctly. Nevertheless, defect's width can be approximately categorized based on the damage intensity. Fatigue cracks were characterized by Ahmad *et al*. (2015) based on metal magnetic memory (MMM) method combined with MFL method. In addition, the correlation between crack growth rate and magnetic flux leakage was obtained. In order to develop a tunnel magneto-resistive (TMR) sensor, Wu *et al*. (2015) performed a 2D stationary numerical simulation using COMSOL Multiphysics 4.2 commercial software. In their simulation, four parameters were considered; coil's lift off, thickness of coil, height of coil and distance between two coils. Based on their numerical simulation, an apparatus was made and its reliability was confirmed by obtained results. Li *et al*. (2007) performed a three-dimensional (3D) stationary numerical simulation in case of multidirectional cracks in specimen and later on they compared numerical simulation results with experimental results. Based on the numerical results, they suggested that, multidirectional sensing setup can be an accurate experimental setup in case of cracks with no specific propagation direction. De Alcantara *et al*. (2015) performed 3D stationary FEA and then compared the results with the experimental one. According to 3D stationary FEA, they obtained effective coil inductance, voltage, resistance and phase angle with respect to different positions of sensor. In their paper, main objective of the numerical simulation was to understand the electromagnetic phenomena and predict sensor's behavior experimentally when it is used to identify mass loss caused by corrosion in steel bars. Liu *et al*. (2018) designed a new type of MFL sensor capable of detecting surface and internal flaws using biased pulse current as the source of magnetic field. They used commercial numerical analysis software to perform stationary simulation of unsaturated and near-saturated magnetization state of a defective cable. Based on their numerical and experimental results, both surface and internal defects can be detected. However, to obtain MFL numerically, they defined a reference line instead of modeling coil sensor itself.

Main focus of previous numerical studies related to damage detection with MFL method was to obtain MFL of a defected specimen right above the defected area using reference line, while coil sensor itself and current induction were disregarded. Consequently, conventional numerical simulation method only provides information about MFL. On the other hand, potential difference caused by MFL is obtained in magnetic sensor apparatus. Thus, comparing conventional numerical analysis with experimental test results might be imprecise.

To overcome this drawback, it was proposed to perform a time dependent numerical simulation by considering specimen's dynamic motion (instead of stationary case), saturation status based on magnetic hysteresis curve (BH curve) in time domain and specific geometry for coil sensor (instead of just a reference line). It can be argued that stationary simulation can reduce analysis time significantly, and therefore, time dependent simulation might be unnecessary. However, it must be noted that if time parameter is ignored, the electromotive force (i.e., induced voltage) induced by variation of magnetic field in time domain (governed by faraday's law of induction), is simply neglected and as a result, no voltage induction is occurred. Hence, in this 2D axisymmetric time dependent study, instead of obtaining MFL as the output signal, induced voltage in coil sensor was directly obtained. To indicate the impact of saturation status of sample on the output signal, numerical simulation was conducted for both saturated and unsaturated specimens. Finally, a comparison between numerical and experimental test results was made to confirm reliability and precision of numerical method. Contents of this research were put in order as follows. Theoretical background is explained in section 2. A detailed explanation of numerical simulation is provided in section 3. In section 4, an experimental test is performed based on an exclusive prototype MFL coil sensor setup in order to evaluate the results of numerical study and lastly, conclusions are given in the section 5.

2. Theoretical background of MFL inspection method

2.1 Basic principle of MFL sensing for metal damage detection

MFL is an NDT method which requires a uniformly distributed magnetic field in order to magnetize specimen completely up to saturation point. When a ferromagnetic specimen is magnetized up to near saturation point, magnetic flux will start leaking out of specimen into air as soon as defect (breakage, cross-sectional loss, etc.) appears in specimen (Xu *et al*. 2012). As a result, by mounting a magneto-sensitive sensor into inspection setup, leaked out flux can be detected and then can be transferred into a storable data for further processing. Based on the fundamentals of MFL testing method, small surface defects such as crack and notch can be detected by hall-effect sensor, while cross-section damages such as cross-section loss due to corrosion, spalling, etc., (whether internally or externally) can be identified by coil sensor. Figs. 1(a)-(b) demonstrate MFL phenomenon for both intact and defected specimens with a step-wise cross section reduction.

Unlike stationary numerical simulations which commonly time dependency is not considered, here, it was tried to accomplish numerical study with almost the same conditions as actual experimental test that includes parameters such as time (i.e., considering Faraday's law of induction and therefore, considering any changes in the induced voltage caused by changes in magnetic flux density), specimen's motion and specimen's saturation status. Hence, all numerical models were simulated by considering magnetization status of the specimen based on its BH curve instead of defining a constant value of relative permeability which provides no saturation limitation. For instance, if only constant relative permeability is taken into account rather than BH curve, by increasing magnitude of magnetic flux density even beyond the saturation point of specimen, induced magnetization value will be much larger

(a) Flawless specimen (b) Defected specimen

Fig. 1 Magnetic flux leakage phenomenon schematically

than it supposed to be without any sign of saturation.

Thus, this study offers a novel FEA which not only takes advantage of BH curve characteristic, also considers magnetization and induced current in time domain while specimen is moving.

2.2 Analytical formulation

Due to electromagnetic phenomenon, in case of MFL system, Maxwell's equations are applicable for performing precise analysis for surrounding magnetic field. Generally, governing Maxwell's equation in case of MFL system in time domain can be written as (Li *et al*. 2007, Jamia *et al*. 2018)

$$\nabla \times H = J; \qquad \nabla \times E = -\frac{\partial B}{\partial t}; \qquad \nabla . B = 0 \tag{1}$$

where, H, J, E and B represent magnetic field intensity, current density, electric field intensity and magnetic flux density, respectively. In this study magnetic field was generated using couple of permanent magnets, hence except for coil sensor and specimen, electric current term can be disregarded from equation. Furthermore, it is possible to define a magnetic scalar potential as well. Simplified Maxwell's equation in case of no electric current can be found as below (Li *et al*. 2007)

$$\mathrm{B} = \mu_0 \mu_r H + B_r; \qquad \nabla \times H = 0; \qquad H = -\nabla V_m \tag{2}$$

where, μ_0 is absolute permeability of vacuum ($\mu_0 = 4\pi \times 10^{-7}\ H/m$), μ_r is relative permeability of materials, B_r is remanent magnetic flux density (where there is no magnetic field, it is representative of magnetic flux density) and V_m is magnetic scalar potential. In case of analyzing coil sensor and specimen, current density cannot be disregarded. Hence, following formulas can be used for coil sensor and conductive specimen (Jamia *et al*. 2018).

$$\nabla \times H = J; \qquad B = \nabla \times A; \qquad E = -\nabla V - \frac{\partial A}{\partial t} \tag{3}$$

Where, A is magnetic vector potential and V is electric scalar potential. Based on electromagnetism theory (i.e., Faraday's law of induction), for multi-turn coil, potential difference and externally generated current density are obtained based on following formulas (Shi *et al*. 2015)

$$V_c = -N\frac{d\emptyset(t)}{dt}; \qquad J_e = \frac{NI_{coil}}{A_c} \tag{4}$$

where, V_c is induced voltage inside coil sensor, N represents number of wire loops in coil sensor, J_e externally generated current density, I_{coil} is total electric current, $\frac{d\emptyset(t)}{dt}$ is the variation of magnetic flux and A_c is cross section area of the coil. Thus, induced voltage in coil sensor generated by MFL due to the presence of defect, can be calculated using Eq. (4).

3. Time dependent numerical simulation of MFL sensor for metal damage detection

3.1 FEA simulation platform

In order to achieve an accurate simulation that can be a good representative of real case, almost all parameters must be considered exactly or at least close to the exact measured value obtained by experimental tests. In addition, performing an accurate FEA requires a strong finite element software capable of performing multiple parametric study at once and more importantly, coupling multiple different physics; for instance, in this study, it was required to perform a numerical study while electromagnetic parameters of magnetic sensor and specimen's motion are considered together and their effects on each other are included as well. Therefore, for this particular study case, COMSOL Multiphysics commercial software was chosen as the FEA software because it allows variety of adjustments and it is capable of performing multi-physics analysis simultaneously.

Although applying parametric study on a 3D domain will lead to better illustration of real case in terms of different defect size and shape, still due to significantly large number of meshes in comparison with 2D case, and also for saving valuable computational time, 2D axisymmetric study in time domain was chosen.

3.2 Target MFL device and specimen

To construct an accurate simulation model, material properties of actual sensor and specimen must be chosen correctly. According to the actual magnetic sensor device, two low carbon steel belts were used as two ferromagnetic yokes, which had been embedded symmetrically inside an aluminum frame as shown in Fig. 2(1). In each yoke, there were six neodymium permanent magnets that were distributed symmetrically in each side of yokes with magnetic flux density of each magnet equal to 1 Tesla. This probe had a detecting coil sensor with 10 turns of copper

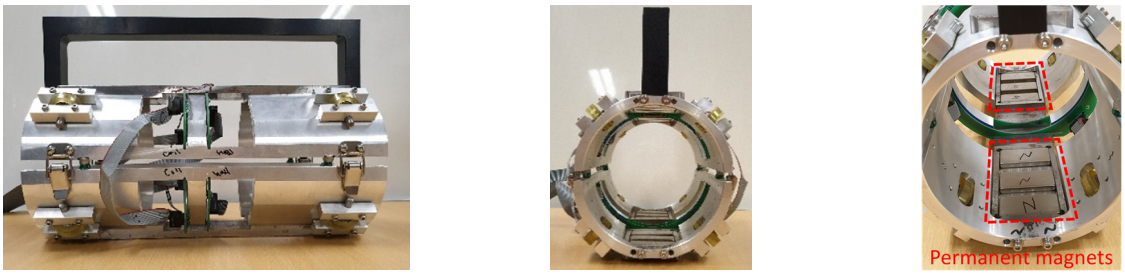

(a) Magnetic sensor apparatus

(b) Steel rod specimen

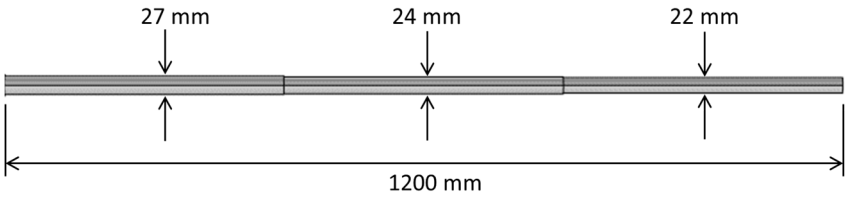

(c) Schematic view of specimen

Fig. 2 Experimental test setup

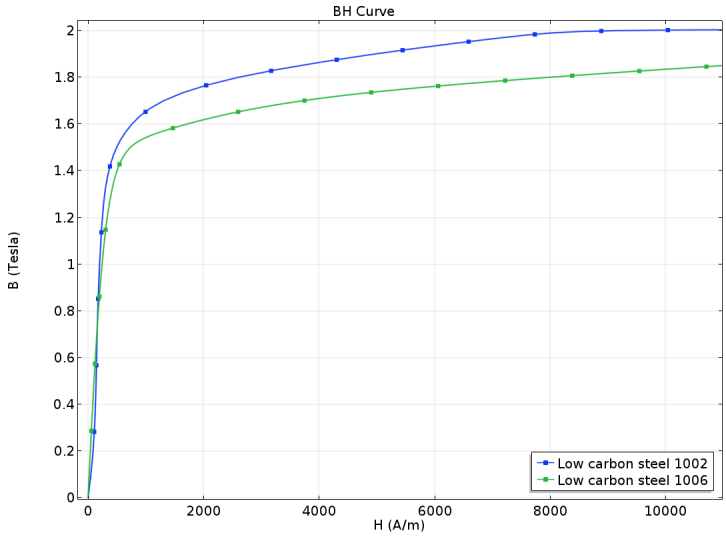

Fig. 3 B-H curve of ferromagnetic handles and specimen

wire which were printed on a circuit board. This sensing coil was located in the middle of yoke. The sensing probe was designed to detect defects (surface and subsurface defects) in variety of ferromagnetic samples with different sizes such as steel pipes and steel cables. A specimen used in this study was an ordinary construction steel rod with saturation point approximately equal to 1.4 to 1.5 Tesla. The specimen had two cross sectional reductions, and each cross section reduction was made with 40 cm gap from the next one. First and second cross-section reductions were made into the specimen uniformly by reducing diameter in each section from initial value of 27 mm to 24 and 22 mm, respectively. Thus, reduction percentages of first and second cross-section were equal to 21% and 16%, respectively.

3.3 Simulation parameters

In order to assign proper materials for numerical simulation model, low carbon steel 1006 and low carbon steel 1002 were chosen as specimen and ferromagnetic handles, respectively. Furthermore, associated BH curves of low carbon steel 1002 and 1006 are plotted in Fig. 3.

In term of simulating specimen's motion, for avoiding any complexity, a constant velocity for specimen must be

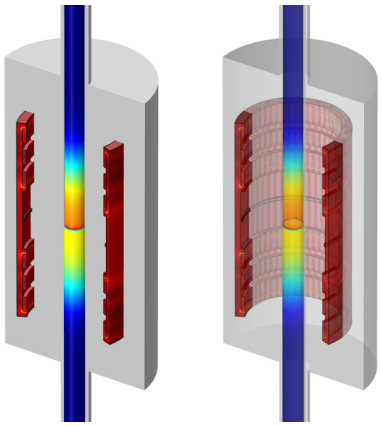

Fig. 4 Air boundary in grey color

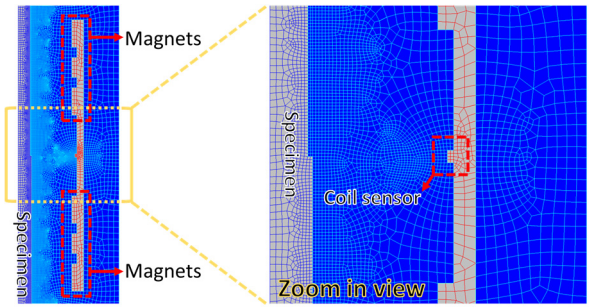

Fig. 5 Meshed geometries and magnetic sensor

taken into account. To achieve this goal in case of numerical study, motion of any specific sub-domain can be defined accurately by using deformed geometry physic. Therefore, specimen's pace for numerical study was assumed to be equal to 20 cm/s (same pace as experimental test).

It should be indicated that parameters such as permanent magnets lift-off, coil sensor lift-off, magnitude of the magnetic flux density, and the distance between permanent magnets in each yoke can affect the output signal of sensing coil. To perform a precise numerical analysis, these effective factors were assumed to have constant values for both numerical and experimental analyses.

In experimental test, magnetic field was not affected by the surrounding air due to its relative permeability which is almost equal to 1 and magnetic field can pass through it without any disturbance. Consequently, in FEA, surrounding material was defined as air with relative permeability of 1. By doing so, magnetic field is not affected by surrounding air, but only affected by ferromagnetic handle and specimen. The surrounding air domains modeled in the FE model were shown in Fig. 4.

Numerical simulation must be accompanied with the optimum mesh size and time intervals to eliminate any chance of inaccurate results and excessive simulation time. Thus, quadrilateral mesh element was chosen to mesh geometry with maximum and minimum size equal to 4 mm and 1 mm respectively. Fig. 5 illustrates meshed specimen along with magnetic yoke. Finally, time dependent study was applied with 10 milliseconds time interval.

3.4 Numerical simulations of saturated and unsaturated specimen

As mentioned in Section 2.1, based on MFL's fundamental principle, specimen must be near saturation point so that magnetic flux can leak out of the specimen and can be detected by proper sensor (Xu *et al*. 2012). In this section, the importance of saturation status of sample was investigated numerically. Therefore, as it is shown in Fig. 6(a), a reference line was defined to acquire saturation status of specimen in middle of the steel rod. It can be observed that in Fig. 6(b), magnetization level inside specimen exposed to weaker magnetic field (i.e., 0.28 Tesla), was not strong enough to saturate specimen (magnetization is less than 0.8 Tesla), while magnetization of the specimen exposed to stronger magnetic field (i.e., 1 Tesla) was almost equal to 1.8 Tesla, which is well beyond the saturation point of low carbon steel 1006 (i.e., 1.4 Tesla); as a result, it can be noted that specimen was saturated.

To compare between saturated and unsaturated cases while specimen is subjected to a motion with constant velocity equal to 20 cm/s, numerical time dependent simulation was performed for two different magnitude of magnetic flux density; 0.28 and 1 Tesla. Figs. 7(a)-(b) demonstrate axial component of induced magnetic flux density inside specimen. It is indicated that, the specimen exposed to permanent magnets with magnetic flux density

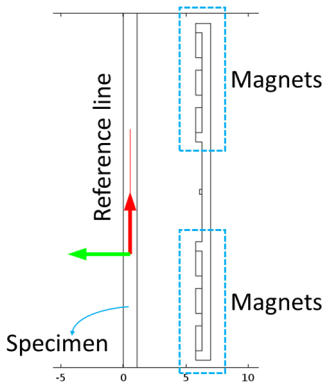

(a) Reference line in red color

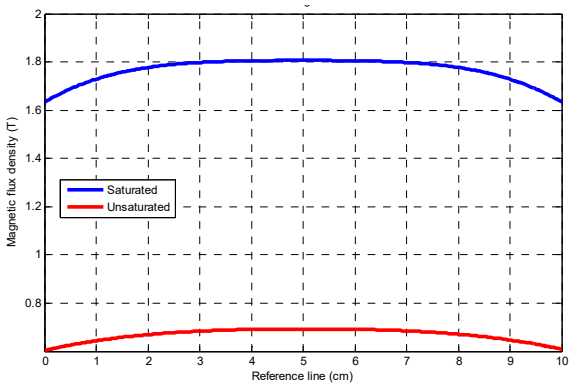

(b) Saturation status of specimen across the reference line

Fig. 6 Specimen's saturation status

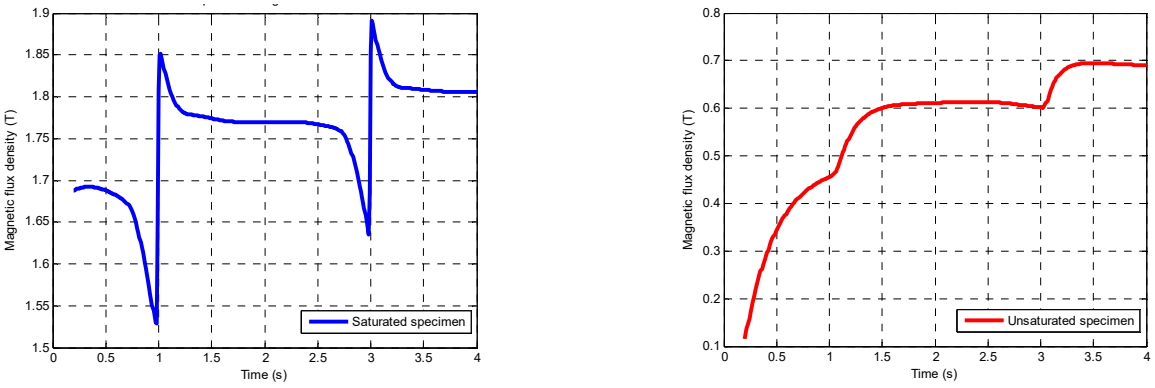

(a) Axial component of magnetic flux density (saturated specimen) (b) Axial component of magnetic flux density (unsaturated specimen)

Fig. 7 Induced magnetization during a complete inspection

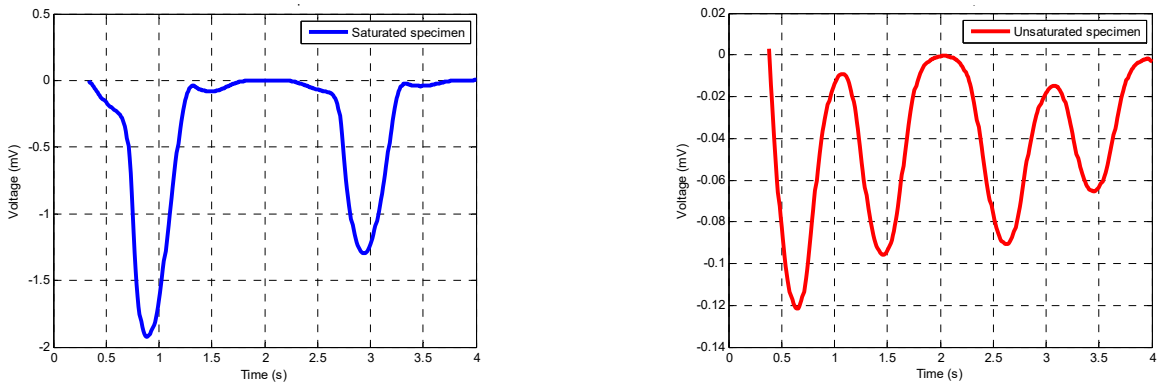

(a) Axial component of magnetic flux density (saturated specimen) (b) Axial component of magnetic flux density (unsaturated specimen)

Fig. 8 Coil sensor's signal of numerical simulation

equal to 1 Tesla was completely saturated. On the other hand, the specimen pushed through magnetic field which was generated by 0.28 Tesla permanent magnets, was not saturated and axial component of magnetic flux density was well below saturation (i.e., based on Fig. 3, saturation point of low carbon steel 1006 is around 1.5 T). Moreover, it can be realized that if specimen is not saturated, by pushing specimen with a constant velocity inside magnetic field, it leads to change in magnitude of induced magnetization not only in the location of flaw, also in vicinity of the flaw as well. Initially, gradient of induced magnetization increased and when cross section loss approached sensing coil, gradient decreased. This increase and decrease behavior of gradient happened again when defected section of specimen passed from the other side of sensing coil. However, if specimen is saturated, magnetic flux density experiences negligible changes in flawless segments of specimen. Fig. 7(a) shows gradient of induced magnetization experienced a sharp increase when cross section loss of specimen just reached the sensing coil.

For unsaturated specimen, in each cross section loss, gradient of induced magnetization changes two times while for saturated specimen, in each cross section loss, gradient change occurs only once with noticeable pulse-shape behavior. This difference will have a significant effect on the coil sensor output signal as it will be explained in next section.

3.5 Numerical simulation of moving specimen for defect detection

In this section of numerical simulation, coil sensor's output signal was obtained. According to output signals of coil sensor shown in Figs. 8(a)-(b), both saturated and unsaturated cases demonstrated different behaviors; output signal in saturated case had only one peak corresponding to each defect due to the fact that in a saturated specimen, when the magnitude of magnetic field increases, the magnetization will remain almost the same (Fig. 3). Therefore, initially there is no induced voltage inside coil sensor until specimen's defect approaches the coil sensor, from this point, magnitude of induced voltage inside coil starts increasing considerably fast until it reaches to its maximum value as soon as defect reaches coil sensor. When cross-section reduction segment has just passed the coil sensor, magnitude of output voltage starts decreasing remarkably until it reaches to minimum value again. In case of induced voltage in coil sensor for unsaturated specimen, instead of a sharp one-peak behavior, two peaks and a local trough can be observed. The main reason of this particular behavior can be explained using Fig. 7, which is having two curvy steps rather than two sharp pulse-shape peaks in magnetization plot. Based on the obtained results, unsaturated sample have a negligible flux leakage, while for saturated sample significant flux leakage can be observed

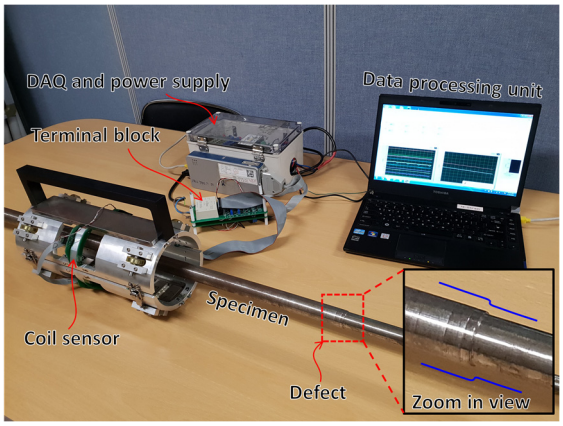

Fig. 9 Experimental test setup along with steel specimen

and detected.

4. Experimental validation

In this section, it was tried to explain about experimental test setup and after that a comparison was made between numerical simulation results and experimental output results to validate accuracy and reliability of the numerical method. Fig. 9 shows the experimental test setup that was constructed based on numerical model along with a steel specimen with same measurement and defect size as numerical model. To conduct an inspection, specimen was manually pushed inside the inspection apparatus, and consistency of inspection pace was checked and confirmed. Moving speed of the sample was the same as the one in the numerical simulation. The sensor probe includes a 10 loops of copper wire printed on circuit board, 12 permanent magnets each capable of generating 1 Tesla flux density, an aluminum frame, a pair of low carbon steel yokes and a data acquisition (DAQ) unit. The DAQ unit used in this study was an NI cDAQ-9181 Ethernet compact data acquisition chassis with a NI 9205 analog input module and sampling rate was set as 500 Hz. To adjust the linear trend of the signal manually, a terminal circuit board was placed between the coil sensor and the DAQ unit. It should be noted that, to validate numerical simulation, experimental test was repeated three time with same parameters as numerical simulation such as specimen's pace and sensor's parameters (e.g., coil sensor's lift off, magnet's strength, etc.). Also, saturation status of specimen was measured by a magnetometer and it was confirmed that magnetization level has reached to saturation. In order to observe changes in the coil sensor's signal clearly, output data was integrated by circuit board automatically. Benefit of having an integration circuit board is all defects have their own specific signature in output signal no matter what size and shape they have, also it makes detection relatively easy due to the fact that instead of having a sharp pulse in output signal (just like the saturated results in simulation), an integrated form of data is appeared in output plot. More importantly, amplitude of the integrated output signal is not dependent on the velocity of sample. Thus, according to Fig. 10, as soon as flaw approaches to the coil sensor,

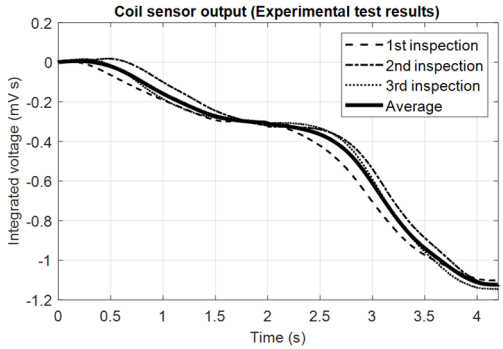

Fig. 10 Coil sensor's signal obtained from experimental apparatus

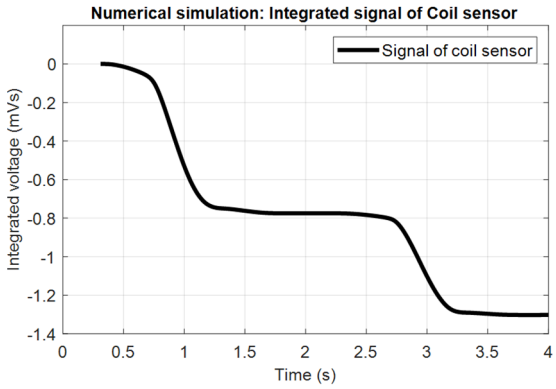

Fig. 11 Integrated signal of Coil sensor obtained from numerical simulation

output signal starts increasing and reaches to maximum value when defect is traversing inside coil sensor.

Figs. 10 and 11 illustrate coil's output signal using experimental test setup and numerical simulation, respectively. According to integrated output signal obtained by numerical simulation and experimental test in case of saturated specimen, same signal with stepwise pattern can be observed. Fig. 11 shows that the first cross-sectional reduction flaw was detected by change in signal amplitude slightly larger than the second cross-section reduction flaw (due to the fact that first cross-sectional creates larger area loss).

Although the pattern of integrated signals of numerical simulation and experimental inspection were the same, yet amplitude changes in the signals related to stepwise cross section reduction were not equal. Experimental result showed larger signal amplitude change in case of second flaw while in numerical simulation it was the opposite. It can be argued that, the first defect must induce more voltage change with respect to the second defect, because first flaw creates larger area loss and accordingly higher flux leakage. This behavior which happened in experimental test, can be occurred by partially magnetized specimen or impurity of material used in specimen. If a sample contains impurity, magnetization level in the area with impurity is decreased, and therefore, flux leakage will be decreased as well. Partially magnetized sample is referred to a sample when magnetization is not uniform across the region of interest. Generally, when a steel sample

is exposed to a considerably strong magnetic field, it can be permanently magnetized. This exposure can be either unwanted contact between sample and magnet or repeating experimental test in one direction for several times. If a permanently magnetized sample is exposed to a weaker magnetic field (or same magnetic field but with larger lift-off from magnets), specimen will not be magnetized uniformly, and partial magnetization will occur. This partially magnetization causes the difference between the output signal of numerical simulation and experimental tests.

5. Conclusions

In this study, it was tried to achieve highly accurate numerical simulation in damage detection using coil sensor based on MFL testing principle. By having a numerical method capable of representing experimental test, not only an optimum device for any particular test can be obtained, but also unexpected results which may cause by limitation of MFL method (e.g., partially magnetized specimen) can be interpreted. To do that, a novel FEA was proposed which unlike previous researches, saturation status of specimen and dynamic motion of specimen were taken into account, also coil sensor's geometry was modeled in simulation as well. Consequently, a realistic time dependent simulation was performed and corresponding output signal was acquired. According to numerical results, when specimen was not saturated, two local peaks behavior happened, while in case of saturated specimen, one peak behavior happened (when only one cross-sectional defect is inspected). To validate the proposed numerical method, experimental tests were also conducted in this study. For making a comparative study between numerical and experimental study, an additional signal processing by integrating output signal of numerical simulation was performed. According to both integrated numerical and experimental results in case of saturated specimen, an acceptable accuracy was observed and performance of numerical simulation in case of time dependent simulation with considering all vital parameters such as saturation status and equation of motion was confirmed. As it was mentioned in the context, partially magnetization and impurity of specimen can have considerable effects on coil sensor's signal. Also having an optimized magnetic probe for conducting experimental test is essential. Thus, these effects must be investigated in future works.

Acknowledgments

This research was supported by a grant (19CTAP-C151927-01) from the Transportation Technology Promotion Research Program funded by the Ministry of Land, Infrastructure and Transport of the Korean government.

References

COMSOL (2017), COMSOL AC/DC Module user's guide, COMSOL, Inc., Los Angeles, CA, USA

Ahmad, M., Arifin, A., Abdullah, S., Jusoh, W. and Singh, S. (2015), "Fatigue crack effect on magnetic flux leakage for A283 grade C steel", *Steel Compos. Struct., Int. J.*, **19**(6), 1549-1560. https://doi.org/10.12989/scs.2015.19.6.1549

Banjara, N.K., Sasmal, S. and Srinivas, V. (2019), "Damage progression study in fibre reinforced concrete using acoustic emission technique", *Smart Struct. Syst., Int. J.*, **23**(2), 173-184. https://doi.org/10.12989/sss.2019.23.2.173

Caesarendra, W., Kosasih, B., Tieu, A.K., Zhu, H., Moodie, C.A. and Zhu, Q. (2016), "Acoustic emission-based condition monitoring methods: Review and application for low speed slew bearing", *Mech. Syst. Signal Process.*, **72**, 134-159. https://doi.org/10.1016/j.ymssp.2015.10.020

Dai, D. and He, Q. (2014), "Structure damage localization with ultrasonic guided waves based on a time–frequency method", *Signal Process.*, **96**, 21-28. https://doi.org/10.1016/j.sigpro.2013.05.025

de Alcantara, N.P., da Silva, F.M., Guimarães, M.T. and Pereira, M.D. (2015), "Corrosion assessment of steel bars used in reinforced concrete structures by means of eddy current testing", *Sensors*, **16**(1), 15. https://doi.org/10.3390/s16010015

Elliott, M.E. and Heymsfield, E. (2003), "Inspection of Luling bridge cable stays: Case study", *J. Constr. Eng. Manage.*, **129**(2), 226-230. https://doi.org/10.1061/(ASCE)0733-9364(2003)129:2(226)

Feng, Q., Li, R., Nie, B., Liu, S., Zhao, L. and Zhang, H. (2017), "Literature review: theory and application of in-line inspection technologies for oil and gas pipeline girth weld defection", *Sensors*, **17**(1), 50. https://doi.org/10.3390/s17010050

Garg, M., Sharma, S., Sharma, S. and Mehta, R. (2016), "Non-contact damage monitoring technique for FRP laminates using guided waves", *Smart Struct. Syst., Int. J.*, **17**(5), 795-817. https://doi.org/10.12989/sss.2016.17.5.795

Gomez, C.Q., Garcia, F.P., Arcos, A., Cheng, L., Kogia, M. and Papelias, M. (2017), "Calculus of the defect severity with EMATs by analysing the attenuation curves of the guided waves", *Smart Struct. Syst., Int. J.*, **19**(2), 195-202. https://doi.org/10.12989/sss.2017.19.2.195

Iqbal, H., Tesfamariam, S., Haider, H. and Sadiq, R. (2017), "Inspection and maintenance of oil & gas pipelines: a review of policies", *Struct. Infrastruct. Eng.*, **13**(6), 794-815. https://doi.org/10.1080/15732479.2016.1187632

Jain, A. and Sharma, S. (2016), "Monitoring degradation in concrete filled steel tubular section using guided waves", *Smart Struct. Syst., Int. J.*, **19**(4), 371-382. https://doi.org/10.12989/sss.2017.19.4.371

Jamia, N., Friswell, M.I., El-Borgi, S. and Fernandes, R. (2018), "Simulating eddy current sensor outputs for blade tip timing", *Adv. Mech. Eng.*, **10**(1), 1-12. https://doi.org/10.1177/1687814017748020

Kim, J.-W. and Park, S. (2018), "Magnetic flux leakage–based local damage detection and quantification for steel wire rope non-destructive evaluation", *J. Intell. Mater. Syst. Struct.*, **29**(17), 3396-3410. https://doi.org/10.1177/1045389X17721038

Kim, J.-M., Lee, J. and Sohn, H. (2018a), "Detection of tension force reduction in a post-tensioning tendon using pulsed-eddy-current measurement", *Struct. Eng. Mech., Int. J.*, **65**(2), 129-139. https://doi.org/10.12989/sem.2018.65.2.129

Kim, J., Park, M., Park, S. and Kim, J. (2018b), "Improvement of MFL sensing–based damage detection and quantification for steel bar NDE", *Smart Struct. Syst., Int. J.*, **22**(2), 239-247. https://doi.org/10.12989/sss.2018.22.2.239

Kuang, K., Li, D. and Koh, C. (2016), "Acoustic emission source location and noise cancellation for crack detection in rail head", *Smart Struct. Syst., Int. J.*, **18**(5), 1063-1085.

https://doi.org/10.12989/sss.2016.18.5.1063
Li, Y., Wilson, J. and Tian, G.Y. (2007), "Experiment and simulation study of 3D magnetic field sensing for magnetic flux leakage defect characterisation", *NDT & E Int*., **40**(2), 179-184. https://doi.org/10.1016/j.ndteint.2006.08.002
Liu, X., Xiao, J., Wu, B. and He, C. (2018), "A novel sensor to measure the biased pulse magnetic response in steel stay cable for the detection of surface and internal flaws", *Sensors Actuators A*: *Phys*., **269**, 218-226. https://doi.org/10.1016/j.sna.2017.11.005
Mehrabi, A.B. and Farhangdoust, S. (2018), "A Laser-Based Noncontact Vibration Technique for Health Monitoring of Structural Cables: Background, Success, and New Developments", *Adv*. *Acoust*. *Vib*., 2018. https://doi.org/10.1155/2018/8640674
Munoz, V., Vales, B., Perrin, M., Pastor, M.-L., Welemane, H., Cantarel, A. and Karama, M. (2016), "Damage detection in CFRP by coupling acoustic emission and infrared thermography", *Compos*. *Part B*: *Eng*., **85**, 68-75. https://doi.org/10.1016/j.compositesb.2015.09.011
Rifai, D., Abdalla, A.N., Razali, R., Ali, K. and Faraj, M.A. (2017), "An eddy current testing platform system for pipe defect inspection based on an optimized eddy current technique probe design", *Sensors*, **17**(3), 579. https://doi.org/10.3390/s17030579
Rocha, T.J., Ramos, H.G., Ribeiro, A.L. and Pasadas, D.J. (2015), "Magnetic sensors assessment in velocity induced eddy current testing", *Sensors Actuat*. *A*: *Phys*., **228**, 55-61. https://doi.org/10.1016/j.sna.2015.02.004
Shi, Y., Zhang, C., Li, R., Cai, M. and Jia, G. (2015), "Theory and application of magnetic flux leakage pipeline detection", *Sensors*, **15**(12), 31036-31055. https://doi.org/10.3390/s151229845
Strantza, M., Van Hemelrijck, D., Guillaume, P. and Aggelis, D.G. (2017), "Acoustic emission monitoring of crack propagation in additively manufactured and conventional titanium components", *Mech*. *Res*. *Commun*., **84**, 8-13. https://doi.org/10.1016/j.mechrescom.2017.05.009
Sun, Y., Liu, S., Deng, Z., Tang, R., Ma, W., Tian, X., Kang, Y. and He, L. (2018), "Magnetic flux leakage structural health monitoring of concrete rebar using an open electromagnetic excitation technique", *Struct*. *Health Monitor*., **17**(2), 121-134. https://doi.org/10.1177/1475921716684340
Wandowski, T., Malinowski, P. and Ostachowicz, W. (2016), "Circular sensing networks for guided waves based structural health monitoring", *Mech*. *Syst*. *Signal Process*., **66**, 248-267. https://doi.org/10.1016/j.ymssp.2015.05.001
Wu, B., Wang, Y., Liu, X. and He, C. (2015), "A novel TMR-based MFL sensor for steel wire rope inspection using the orthogonal test method", *Smart Mater*. *Struct*., **24**(7), 075007. https://doi.org/10.1088/0964-1726/24/7/075007
Wu, J., Fang, H., Huang, X., Xia, H., Kang, Y. and Tang, C. (2017a), "An Online MFL Sensing Method for Steel Pipe Based on the Magnetic Guiding Effect", *Sensors*, **17**(12), 2911. https://doi.org/10.3390/s17122911
Wu, J., Fang, H., Li, L., Wang, J., Huang, X., Kang, Y., Sun, Y. and Tang, C. (2017b), "A lift-off-tolerant magnetic flux leakage testing method for drill pipes at wellhead", *Sensors*, **17**(1), 201. https://doi.org/10.3390/s17010201
Xu, J., Wu, X., Cheng, C. and Ben, A. (2012), "A magnetic flux leakage and magnetostrictive guided wave hybrid transducer for detecting bridge cables", *Sensors*, **12**(1), 518-533. https://doi.org/10.3390/s120100518